Proc. Natl. Acad. Sci. USA
Vol. 92, pp. 1826–1830, March 1995
Biophysics

Femtosecond infrared spectroscopy of reaction centers from *Rhodobacter sphaeroides* between 1000 and 1800 cm^{-1}

(photosynthesis/bacterial reaction centers/time-resolved infrared spectroscopy)

P. HAMM†, M. ZUREK†, W. MÄNTELE‡, M. MEYER§, H. SCHEER§, AND W. ZINTH†¶

†Institut für Medizinische Optik der Ludwig-Maximilians-Universität München, Barbarastrasse 16, 80797 Munich, Germany; ‡Albert-Ludwigs-Universität Freiburg, Albert-Strasse 23, 79104 Freiburg, Germany; and §Botanisches Institut der Ludwig-Maximilians-Universität München, Menzinger Strasse 67, 80638 Munich, Germany

Communicated by Wolfgang Kaiser, Technische Universitat München, Garching, Germany, November 9, 1994

ABSTRACT **Time-resolved pump-and-probe experiments of reaction centers of the purple bacterium *Rhodobacter sphaeroides* (R26) in the mid-IR region between 1000 and 1800 cm^{-1} are recorded with a time resolution of 300–400 fs. The difference spectra of the states P*, $P^+H_A^-$, and $P^+Q_A^-$ with respect to the ground state P predominantly reflect changes of the special pair. They show positive and negative bands due to changes of distinct vibrational modes superimposed on a broad background of enhanced absorption. A number of certain bands can be assigned to the special pair P, to the bacteriopheophytin H_A, and to the quinone Q_A. The temporal evolution of the IR absorbance changes is well described by the time constants known from femtosecond spectroscopy of the electronic states. Differences occur only at very early times, which are indicative of fast vibrational relaxation with a time constant of a few hundred femtoseconds.**

In the reaction center (RC) of the photosynthetic bacterium *Rhodobacter sphaeroides*, excitation by light initiates electron transfer (ET) reactions along a chain of chromophore molecules. ET starts at the primary donor P, a pair of strongly coupled bacteriochlorophyll a (BChl-a) molecules. The electron is subsequently transferred in ≈3.5 ps to an accessory BChl-a molecule, B_A, and in a second rapid transfer step (0.9 ps) to a bacteriopheophytin a (BPhe-a) molecule, H_A. The initial charge separation process is terminated with the transfer of the electron to the quinone Q_A within ≈200 ps (1–6). In isolated RCs, where the secondary quinone Q_B was removed, the charge persists ≈100 ms at Q_A (7). In recent publications, ultrafast spectroscopic techniques probing the electronic absorption bands of the pigments established this stepwise ET scheme and confirmed it by determination of the energy levels of the various intermediate states (8, 9). While basic principles of the ET process are known (10–12), the microscopic understanding of the reaction requires more detailed experimental data for the various intermediate states. Information is especially required that connects the dynamic and spectroscopic properties with data from x-ray structure analysis (13, 14). Detailed quantum chemical calculations of the electronic structure of the ground state of the special pair P, its electronically excited state P*, and the cation P^+ gave valuable information on the high quantum efficiency, the unidirectionality of the ET, and the absorption properties of the RCs. These calculations are mainly based on the spectra deduced from steady-state and time-resolved spectroscopy of electronic states and on the Stark effect (15–18). Additional knowledge is expected if vibrational modes of the RCs are investigated. Important information came from steady-state IR and resonance Raman studies (19–23), allowing assignment of specific vibrational modes to molecular groups. In addition, time-resolved vibrational spectroscopy should allow one to find (*i*) electronic and structural changes of the chromophores and the protein by observation of the position and the strength of vibrational bands as well as (*ii*) the role of vibrational motions for the ET by observation of nonequilibrium vibrational populations.

On the time scale of 100 μs to 1 ms, weak absorption changes were found in the C=O region due to protonation of an amino acid side group near Q_B (24). In a recent publication, transient IR spectra in the range of 1500–1900 cm^{-1} were presented with a time resolution of 60 ps giving information on the intermediates $P^+H_A^-$ and $P^+Q_A^-$ (25). The experiment demonstrated that dynamic changes of the transient spectra induced by the primary ET reaction are essentially completed after several hundred picoseconds. Additional information with higher time resolution in the same spectral range was presented very recently (26).

In the present paper, we present experimental data for the extended spectral range from 1000 to 1800 cm^{-1} taken with a time resolution of better than 400 fs. The data give evidence of molecular changes upon formation of the intermediates P*, $P^+H_A^-$, and $P^+Q_A^-$. The spectral range covers the pigment ester and keto C=O range; the amide C=O region; as well as the frequency range of C—N and C—C stretching and C—H bending modes. Here we focus on presentation of the experimental data combined with a qualitative interpretation of the results.

MATERIALS AND METHODS

RCs from *Rb. sphaeroides* R26 were prepared according to standard procedures (27). The RCs were treated with terbutryn in order to eliminate Q_B; subsequently, they were concentrated to 5 mM with a Centricon 30 ultrafiltration cell (Amicon) and held between two CaF_2 windows, yielding a sample thickness of 10 μm. The measurements with probing wavelengths of >1680 and <1560 cm^{-1} were performed in H_2O buffer (20 mM Tris·HCl/0.08% lauryldimethylamine-*N*-oxide, pH 8). For investigations between 1560 and 1680 cm^{-1}, H_2O was exchanged by ^2H_2O by diluting a concentrated sample once in ^2H_2O followed by a subsequent reconcentration. All experiments were done at 12°C. The transient spectra were recorded as follows: Tunable femtosecond IR probing pulses were generated by difference frequency mixing between the output of an amplified Ti:sapphire laser (λ = 815 nm; repetition rate, 1 kHz) and the output of a traveling wave dye laser in a $AgGaS_2$ crystal as described recently (28). A second traveling wave dye laser delivered excitation pulses at 870 nm with an energy of 1 μJ. Relatively high excitation densities with

The publication costs of this article were defrayed in part by page charge payment. This article must therefore be hereby marked "*advertisement*" in accordance with 18 U.S.C. §1734 solely to indicate this fact.

Abbreviations: RC, reaction center; ET, electron transfer; BChl-a, bacteriochlorophyll a; BPhe-a, bacteriopheophytin a; FT, Fourier transform.

¶To whom reprint requests should be addressed.

approximately one photon absorbed per RC were used. Excitation and probing pulses were polarized parallel to each other. The spectral band width of the IR pulses (65 cm^{-1}) allowed broadband frequency-resolved detection; the IR pulses were dispersed in a grating spectrometer and measured with a 10-element MCT (Grasbey Infrared) detector array with a spectral resolution of 3–8 cm^{-1}. The instrumental response function was determined before each measurement with the help of a thin silicon sample (100 μm thick). Here free carriers are generated by optical excitation leading to induced absorption, which is measured by the IR probing beam. Deconvolution of this signal yields the cross-correlation function of the system, which typically has a width of 300–400 fs (full width at half maximum).

In the experiments presented here, the transient absorbance changes at each point of the spectrum were recorded as a function of the delay time t_D. Transient absorption curves were obtained between 1020 and 1785 cm^{-1}, with a spectral resolution of 3–8 cm^{-1}. The t_D interval from −2 ps to +1 ns was covered by measuring the range from −2 ps to +1 ps in steps of 100 fs and increasing the t_D intervals exponentially between 1 ps and 1 ns. The complete spectra were obtained by combining the individual 10-point spectra at special t_Ds. The accuracy within a 10-element spectrum is better than $\Delta A = 10^{-4}$. Because of inevitable uncertainties upon tuning the laser system, the accuracy between two independent 10-element spectra is of the order of $\Delta A = 3 \times 10^{-4}$ or somewhat larger at the points where the spectra in H_2O and ^2H_2O are connected. The illuminated volume of the sample was completely exchanged between two laser shots by rotating and translating the sample cuvette during the measurement.

The correct ET of the RCs was tested by measuring the decay of P* in a gain experiment at 914 nm. For this purpose, a second probing beam was supplied from a white light continuum. The gain measurement of several sample preparations showed that the decay of P* is not affected by the concentration procedure. A fit of the observed decay of P* yielded a value of 3.2 ± 0.2 ps, which is within the range of values found otherwise (1, 2, 4, 5). We note that these test measurements were performed on the same sample and under the same experimental conditions as the IR measurements.

In frequency-resolved ultrafast spectroscopy, disturbed free induction decay can lead to coherent features, which can pretend absorption changes in excite-and-probe experiments. This phenomenon appears when the dephasing time T_2 of an investigated IR transition line is longer than the duration of the IR probing pulse and when the probing pulse is spectrally resolved (29, 30). According to a theoretical analysis, the coherent signal appears only at negative t_Ds. These effects will be discussed elsewhere.

RESULTS

Temporal Evolution. Four examples of time-resolved IR absorbance changes are shown in Fig. 1 for the frequencies ν_{pr} = 1132 and 1595 cm^{-1} and in Fig. 2 for ν_{pr} = 1443 cm^{-1}. At 1132 cm^{-1}, an instantaneous increase of absorbance at t_D = 0 is followed by a decay, which can be fit well by a single exponential function with a time constant of 3.8 ps. Between 10 ps and 1 ns, a weak increase of absorption is found. Quite different is the situation at 1595 cm^{-1}. There is only a small instantaneous signal followed by a slow absorbance increase, which leads to maximum absorption at ≈10 ps after excitation. Subsequently, the signal decays again until it reaches a constant level at 1 ns. The data can be simulated by assuming an intermediate state increasing with 3.8 ps and decaying with 240 ps. Since the transient absorption change appears simultaneously with the formation of $P^+H_A^-$ and disappears during the ET step to $P^+Q_A^-$, one obviously observes at ν_{pr} = 1595 cm^{-1} an absorption band related to H_A^-. At most other wavelengths,

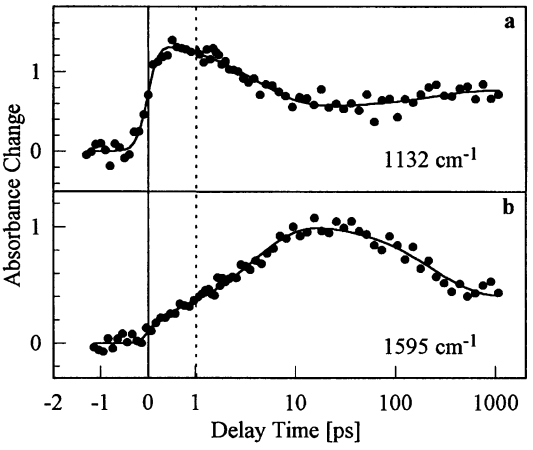

FIG. 1. Transient absorbance changes (×10^3) at 1132 cm^{-1} (*a*) and 1595 cm^{-1} (*b*). Time scale is linear between −2 ps and +1 ps and logarithmic between 1 ps and 1 ns. Model functions (solid lines) in both plots are calculated by using two exponential kinetics with time constants of 3.8 and 240 ps.

the amplitude of the 240-ps kinetic component is 3–5 times smaller than the 3.8-ps component. It turns out that to a first-order description all data measured between 1020 and 1785 cm^{-1} can be explained in the same simple framework. In the present data, there is no evidence for the 0.9-ps kinetic component, which was referred to the fast ET step from $P^+B_A^-$ to $P^+H_A^-$ (5, 6). In addition, no indication for protein motion occurring with a time constant different from those known from visible spectroscopy is found. A global fit of all data yields 3.8 ± 0.4 and 240 ± 40 ps for the time constants of the two kinetics. These values are somewhat smaller than the numbers measured in visible and near-IR experiments but agree within experimental error.

Around t_D = 0, some weak deviations from this simple description are observed. There is evidence for a fast process at early t_Ds, which is most distinct around 1210 and 1440 cm^{-1} (Fig. 2). At this wavelength, the absorption of the RCs (solid circles) clearly increases more slowly than the model curve of the system (dashed line) calculated from the cross-correlation function (deduced from the reference experiment of the silicon sample). A careful inspection of the data supports the notion that there is only a small instantaneous absorption increase followed by an additional increase with a time constant of ≈200 fs. A quantitative analysis of the early time dependence will be given elsewhere.

Transient Absorption Spectra. In Fig. 3 difference spectra are presented for three t_Ds of 1, 10, and 1000 ps. At these t_Ds, high concentrations of single intermediates occur as calculated on the basis of the stepwise ET model (6). Difference spectra taken at these three time points give a general view of the

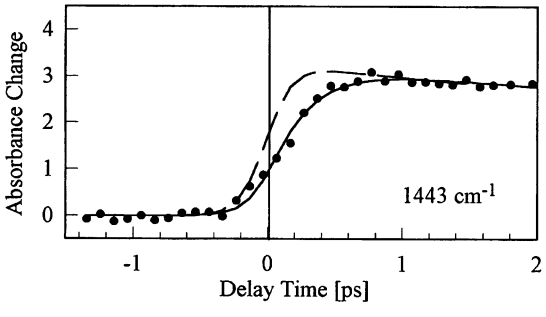

FIG. 2. Transient absorbance changes (×10^3) at 1443 cm^{-1}. Increase of absorption (solid circles) is delayed with respect to the instrumental response function (dashed line), which was calculated considering the reference experiment on silicon.

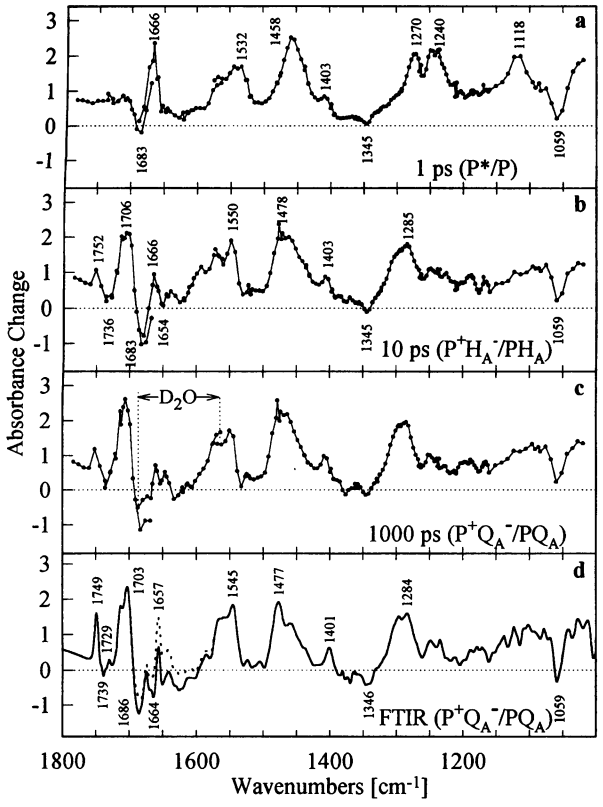

FIG. 3. Transient difference spectra taken 1 (*a*), 10 (*b*), and 1000 (*c*) ps after optical excitation of RCs. Spectra are related to intermediate states P*, $P^+H_A^-$, and $P^+Q_A^-$, respectively. Data are compared with a light-induced steady-state difference spectrum measured in a FTIR spectrometer (*d*). Time-resolved measurements between 1560 and 1710 cm^{-1} are done in ^2H_2O buffer in order to eliminate strong H_2O absorption in this spectral range. FTIR spectrum shows some differences between measurements in H_2O (solid line) and ^2H_2O (dashed line) (20). However, these are broad and do not affect the discussion of narrow bands in the text. Absorbance change is shown $\times 10^3$.

properties of these intermediates. In Fig. 3*a*, t_D = 1 ps is chosen where, according to the stepwise ET model (6), ≈80% of the excited RCs are in state P* (15% are in $P^+B_A^-$ and 5% are in $P^+H_A^-$). At t_D = 10 ps (Fig. 3*b*), >90% are in intermediate $P^+H_A^-$; at t_D = 1 ns (Fig. 3*c*), practically all (>95%) excited RCs have reached $P^+Q_A^-$. For comparison, Fig. 3*d* shows a difference spectrum obtained in a Fourier transform IR (FTIR) experiment by steady state visible illumination (600 nm < λ < 800 nm). This spectrum represents the steady-state accumulation of $P^+Q_A^-$ after complete relaxation. When comparing the spectra of Fig. 3 *c* and *d*, one should keep in mind that in the FTIR spectrum, arbitrary polarization between exciting and probing light was used and that the FTIR spectrum was obtained at a higher spectral resolution (2 cm^{-1}).

The difference spectrum of Fig. 3*a* corresponding to the P → P* excitation shows a number of striking features. Throughout the entire spectral range between 1020 and 1780 cm^{-1} the absorption increases (except at ≈1683 cm^{-1}). In addition, distinct spectral features described by relatively broad positive (1118, 1240, 1270, 1403, 1458, 1532, and 1666 cm^{-1}) and negative (1059, 1345, and 1683 cm^{-1}) bands are superimposed to the increased absorption.

In a similar way, the 10-ps spectrum representing the intermediate state $P^+H_A^-$ shows mainly enhanced absorption and a detailed band pattern. The differences between P* and $P^+H_A^-$ become quite apparent if a double-difference spectrum is calculated (Fig. 4*a*). In this spectrum, representing $A(P^+H_A^-/PH_A) - A(P^*/P)$, a number of negative bands

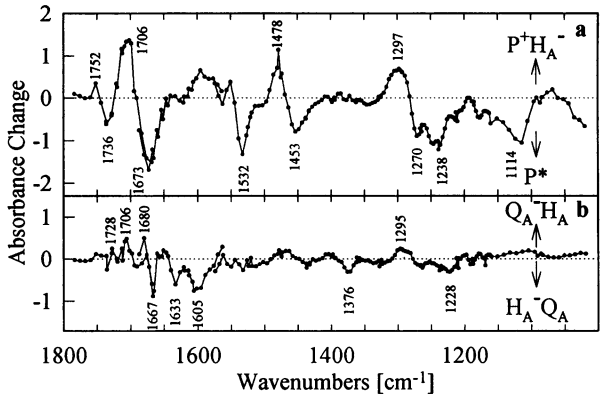

FIG. 4. Difference between the spectra of Fig. 3 *b* and *a* (*a*) and Fig. 3 *c* and *b* (*b*). In the double-difference spectrum in *a* $P^+H_A^-$ bands are positive and P* bands are negative, whereas in *b* Q_A^- and H_A bands are positive and H_A^- and Q_A bands are negative. Absorbance change is shown $\times 10^3$.

appear which indicate that P* has stronger average absorption than $P^+H_A^-$. Prominent features include dispersion-like changes (1673/1706 cm^{-1}, 1736/1752 cm^{-1}), the disappearance of bands (1114, 1238, 1270, 1453, and 1532 cm^{-1}), and the appearance of new bands (1297 and 1478 cm^{-1}).

The changes induced by the transition from $P^+H_A^-$ to $P^+Q_A^-$ are significantly weaker (see double-difference spectrum in Fig. 4*b*). The most evident absorbance changes occur at 1228, 1295, 1376, 1605, 1633, and 1667 cm^{-1}. The two spectra of intermediate $P^+Q_A^-$ recorded at 1 ns and in the FTIR experiment (Fig. 3 *c* and *d*) are comparable. Only weak differences are seen, which originate from the higher spectral resolution of the FTIR measurement. This large similarity of the spectra rules out substantial changes of the structure of the RC after transfer of the electron to the quinone Q_A.

DISCUSSION

Temporal Evolution. The dominant absorption change observed at most wavelengths is an initial absorption increase at t_D = 0 followed by a subsequent 3.8-ps kinetic component. All other kinetic components have smaller amplitudes—i.e., changes of the electronic structure in the special pair upon electronic excitation (absorption change at t_D = 0) or the formation of P^+ (3.8-ps kinetic component) cause the main contribution in the observed IR spectra. Apparently, this property is directly related to the dimeric structure of the electron donor since changes at H_A and Q_A upon reduction are much weaker. The absorption amplitudes from the dimer may be explained by a relatively large change of the π-electron system and the structural conformation of the dimer during the first picosecond after excitation.

While the 3.8- and 240-ps kinetic components are well resolved, the fast ET step from $P^+B_A^-$ to $P^+H_A^-$ in 0.9 ps is not directly seen in the IR data. However, if bands in the B_A/B_A^- difference spectrum are as small as those of the H_A/H_A^- difference spectrum [as suggested by *in vitro* spectra of BChl-a and BPhe-a (31)], it is obvious that a 0.9-ps kinetic component should be very small (≈6 times smaller than the changes shown in Fig. 4*b*, since in the sequential ET model $P^+B_A^-$ is populated to <16%), and a definitive detection is not possible at present.

Recently, vibrational relaxation was discussed in the context of adiabatic and nonadiabatic ET (32, 33). The observation of an oscillating signal in the decay of P* at low temperatures led to the interpretation that coherence may be essential for ET even at room temperature. The excess energy during electronic excitation (estimated from the Stokes shift) can only excite low energy vibrational transitions with ν < 1000 cm^{-1}

not investigated here. Nevertheless, low lying modes of P may be strongly coupled to the observed modes. For example, a displacement of both BChl-a molecules of P with respect to each other is expected to change the electronic distribution in P considerably (17) and should therefore affect the intensity of high-frequency modes. The observed fast transient at 1210 and 1430 cm^{-1} may be explained along this line. This observation indicates that room temperature vibrational relaxation should occur on a time scale of 200 fs, which is clearly faster than the first ET step.

Difference Spectra. The transition from P to P* and the subsequent charge separation modifies the π-electron system of the chromophores involved, changing both the bond strength (shift of a band) and the oscillator strength (change of band intensity). There are two basically different features in the difference spectra, which have to be discussed independently: (*i*) A broad positive absorption background related to P* and P^+ and (*ii*) several narrower positive and negative difference bands from vibrational transitions.

(*i*) The fact that the broad positive absorption appears very fast within 1 ps (Fig. 3*a*) and that it is essentially unchanged until several milliseconds (FTIR spectrum in Fig. 3*d*) supports the notion that it is not caused by thermal effects. Three explanations are offered for the broad absorption background: (*a*) In a charged molecule, positive and negative partial charges may occur, leading to an overall increased dipole moment of the IR transitions with the consequence of a difference spectrum that is mainly positive. This explanation may also be valid in the case of P*, since an asymmetric charge distribution in P* was predicted (15). (*b*) P^+ is known to have a low lying broad electronic transition at 2700 cm^{-1} (16, 17). A similar band was measured in P* (38). Coupling between this transition and the vibrational bands may transfer oscillator strength from the electronic to some vibrational transitions and result in the observed broad absorption increase. (*c*) Due to the complexity of the electronic structure of the RC, it cannot be excluded that there is another low energy electronic transition.

(*ii*) The distinct vibrational bands superimposed to the background give more detailed information. From light-induced steady-state difference spectra and from electrochemically induced difference spectra of RCs and model compounds [isolated BChl-a or BPhe-a molecules in organic solvents in their neutral and radical ion states (31, 34)] a number of assignments have been proposed for the C=O modes of BChl-a and of BPhe-a in the range 1620–1750 cm^{-1}. Reference to these data is made to explain the observed ultrafast absorption changes.

The P* state exhibits a strong positive band at 1666 cm^{-1} and a related negative band at 1683 cm^{-1}. The same negative band is found in the $P^+H_A^-/PH_A$ and the $P^+Q_A^-/PQ_A$ difference spectra with a corresponding positive band at 1706 cm^{-1}. According to ref. 31, this differential band of the primary donor can be assigned to the 9-keto C=O modes [13^1-keto in International Union of Pure and Applied Chemistry (IUPAC) numbering of the atoms] of P_L and P_M (differences between P_L and P_M are not resolved). Therefore, it seems reasonable to relate the 1666/1683 cm^{-1} differential band in the P*/P difference spectrum to a downshift of the same modes. A similar downshift was observed upon formation of the triplet state ^3P (35) pointing to similarities between the electronic structure of P* and ^3P.

Strong coupling of the 10*a* ester C=O bond (13^2 ester in IUPAC numbering) with the π-electron system of ring V is observed for cations or anions of BChl-a or BPhe-a, leading to an upshift of >10 cm^{-1} upon BChl-a cation radical formation or a similar downshift upon BPhe-a anion radical formation (31). In the P^+ spectrum, a difference band due to the 10*a* ester C=O modes at 1752/1736 cm^{-1} is observed (Fig. 3 *b–d*). Since no corresponding feature is observed in the P*/P difference spectrum, we conclude that in P* there is no coupling of this mode with the altered orbital configuration.

Table 1. Band assignments of $Q_A^-H_A/H_A^-Q_A$ double-difference spectrum

Wavelength, cm^{-1}	Sign	Quinone (21)	BPhe (31)
1605	−		
1633	−	Q_A, C=O stretching	
1667	−	Amide I, C=O stretching of Thr M222 near Q_A	
1706	+		H_A, 9-keto C=O
1728	+	COOH, C=O stretching of Glu L104 near Q_A^-	

The 2-acetyl C=O mode (3-acetyl in IUPAC numbering) of P_M is expected around 1654 cm^{-1} (23, 36). In the P* spectrum, there is no signal in this spectral region. However, a small distinct difference band with a negative contribution at 1654 cm^{-1} and a positive contribution at 1666 cm^{-1} is found in the $P^+H_A^-$ spectrum (Fig. 3*b*), which may be associated with the 2-acetyl C=O mode. Probably because of the overlap with quinone bands, this mode does not clearly appear in the $P^+Q_A^-$ spectrum.

Throughout the whole spectral range investigated, the difference spectra at 10 ps ($P^+H_A^-/PH_A$) and at 1000 ps ($P^+Q_A^-/PQ_A$) are quite similar to each other. To suppress the dominant contribution of P^+, a double-difference spectrum is calculated that enhances contributions from Q_A^- and H_A, which are positive, and from H_A^- and Q_A, which are negative (Fig. 4*b*). In the range between 1550 and 1750 cm^{-1}, there are several narrow features that can be compared with bands found in an electrochemically generated Q_A^-/Q_A spectrum (21). The strong negative bands at 1633 and 1667 cm^{-1} as well as the weak positive band at 1728 cm^{-1} were assigned to modes of the quinone Q_A or amino acid side groups near Q_A (for detail see Table 1). Since preliminary H_A^-/H_A difference spectra of RCs of *Rb. sphaeroides* (37) show strong similarities with those from *Rhodopseudomonas viridis*, the remaining bands may also be compared with electrochemically generated *in vitro* BPhe-b^-/BPhe-b spectra (31). The weak positive band at 1706 cm^{-1} can be assigned to the 9-keto C=O mode of BPhe. However, no interpretation for the strong negative band around 1605 cm^{-1} can be given at present.

The lack of detailed assignments of the vibrational modes of BChl-a and BPhe-a in the range <1550 cm^{-1} allows only a brief qualitative discussion of the features observed: P* has strong broadbands around 1530, 1460, and 1250 cm^{-1}—i.e., in the range of C—C and C—N stretching and C—H bending modes. These bands are, at first sight, similar to those observed in the P^+ spectrum. However, a detailed analysis of the double-difference spectrum in Fig. 4*a* shows that these bands are shifted to higher wavenumbers upon the transfer from P* to P^+. Apparently, the bonding strengths of the porphyrin backbone in the electronically excited state P* are weaker than in the cation state.

In conclusion, complete time-resolved IR spectra between 1020 and 1780 cm^{-1} have been measured with a time resolution high enough to resolve the primary reaction steps during bacterial photosynthesis. The data display significant changes in the electronic structure and the vibrational modes of the chromophores in the primary photosynthetic reactions: (*i*) Changes of vibrational modes from the special pair P dominate the difference spectra. (*ii*) The electronically excited P* as well as the cation P^+ show a broad absorption background throughout the spectral range 1000–1800 cm^{-1}. (*iii*) The spectra show narrow differential features in addition to *ii*, with the strongest contribution from the C=O modes (where assignments are straightforward), but also for C—C, C=C, and C—N modes

as well as in the C—H bending region. (*iv*) Additional fast absorbance changes occur on a time scale of vibrational relaxation in 200 fs.

We thank P. Tavan and S. F. Fischer for valuable discussions.

1. Martin, J. L., Breton, J., Hoff, A. J., Migus, A. & Antonetti, A. (1986) *Proc. Natl. Acad. Sci. USA* **83,** 957–961.
2. Breton, A., Martin, J. L., Migus, A., Antonetti, A. & Orzag, A. (1986) *Proc. Natl. Acad. Sci. USA* **83,** 5121–5125.
3. Chan, C.-K., DiMagno, T. J., Chen, L. X.-Q., Norris, J. R. & Fleming, G. R. (1991) *Proc. Natl. Acad. Sci. USA* **88,** 11202–11206.
4. Woodbury, N. W., Becker, M., Middendorf, D. & Parson, W. W. (1985) *Biochemistry* **24,** 7516–7521.
5. Holzapfel, W., Finkele, U., Kaiser, W., Oesterhelt, D., Scheer, H., Stilz, U. & Zinth, W. (1989) *Chem. Phys. Lett.* **160,** 1–7.
6. Holzapfel, W., Finkele, U., Kaiser, W., Oesterhelt, D., Scheer, H., Stilz, U. & Zinth, W. (1990) *Proc. Natl. Acad. Sci. USA* **87,** 5168–5172.
7. Shopes, R. J. & Write, C. A. (1987) *Biochim. Biophys. Acta* **893,** 409–425.
8. Schmidt, S., Arlt, T., Hamm, P., Huber, H., Nägele, T., Wachtveitl, J., Meyer, M., Scheer, H. & Zinth, W. (1994) *Chem. Phys. Lett.* **223,** 116–120.
9. Arlt, T., Schmidt, S., Kaiser, W., Lauterwasser, C., Meyer, M., Scheer, H. & Zinth, W. (1993) *Proc. Natl. Acad. Sci. USA* **90,** 11757–11761.
10. Bixon, M., Jortner, J. & Michel Beyerle, M. E. (1991) *Biochim. Biophys. Acta* **1056,** 301–315.
11. Bixon, M., Jortner, J. & Michel Beyerle, M. E. (1992) in *The Photosynthetic Bacterial Reaction Center*, eds. Breton, J. & Vermeglio, S. (Plenum, New York), pp. 283–290.
12. Marcus, R. A. (1987) *Chem. Phys. Lett.* **133,** 471–477.
13. Deisenhofer, J. & Michel, H. (1989) *EMBO J.* **8,** 2149–2170.
14. Allen, J. P., Feher, G., Yeates, T. O., Komiya, H. & Rees, D. C. (1987) *Proc. Natl. Acad. Sci. USA* **84,** 5730–5734.
15. Scherer, P. O. J. & Fischer, S. F. (1989) *Chem. Phys.* **131,** 115–127.
16. Scherer, P. O. J. & Fischer, S. F. (1992) in *The Photosynthetic Bacterial Reaction Center*, eds. Breton, J. & Vermeglio, S. (Plenum, New York), pp. 193–207.
17. Parson, W. W., Nabedryk, E. & Breton, J. (1992) in *The Photosynthetic Bacterial Reaction Center*, eds. Breton, J. & Vermeglio, A. (Plenum, New York), pp. 79–88.
18. Scherer, P. O. J., Fischer, S. F., Lancaster, C. R. D., Fritsch, G., Schmidt, S., Arlt, T., Dressler, K. & Zinth, W. (1994) *Chem. Phys. Lett.* **223,** 110–115.
19. Mattioli, T. A., Hoffman, A., Robert, B., Schrader, B. & Lutz, M. (1991) *Biochemistry* **30,** 4648–4654.
20. Leonhard, M. & Mäntele, W. (1993) *Biochemistry* **32,** 4532–4538.
21. Bauscher, M., Leonhard, M., Moss, D. A. & Mäntele, W. (1993) *Biochim. Biophys. Acta* **1183,** 59–71.
22. Palaniappan, V., Martin, P., Chynwat, V., Frank, H. A. & Bocian, D. F. (1993) *J. Am. Chem. Soc.* **115,** 12035–12049.
23. Lutz, M. & Mäntele, W. (1991) in *Chlorophylls*, ed. Scheer, H. (CRC, Boca Raton, FL), pp. 855–902.
24. Hienerwadel, R., Thibodeau, D. L., Lenz, F., Nabedryk, E., Breton, J., Kreutz, W. & Mäntele, W. (1992) *Biochemistry* **31,** 5799–5808.
25. Maiti, S., Cowen, B. R., Diller, R., Iannone, M., Moser, C. C., Dutton, P. L. & Hochstrasser, R. M. (1993) *Proc. Natl. Acad. Sci. USA* **90,** 5247–5251.
26. Maiti, S., Walker, G. C., Cowen, B. R., Pippenger, R., Moser, C. C., Dutton, P. L. & Hochstrasser, R. M. (1994) *Proc. Natl. Acad. Sci. USA* **91,** 10360–10364.
27. Beese, D., Steiner, R., Scheer, H., Angerhofer, A., Robert, B. & Lutz, M. (1987) *Photochem. Photobiol.* **47,** 293–304.
28. Hamm, P., Lauterwasser, C. & Zinth, W. (1993) *Opt. Lett.* **18,** 1943–1945.
29. Joffre, M., Hulin, D., Migus, A., Antonetti, A., Guillaume, C. B., Peyghambarian, N., Lindberg, M. & Koch, S. W. (1988) *Opt. Lett.* **13,** 276–278.
30. Cruz, C. H. B., Gordon, J. P., Becker, P. C., Fork, R. L. & Shank, C. V. (1988) *IEEE J. Quantum Electron.* **24,** 261–266.
31. Mäntele, W., Wollenweber, A., Nabedryk, L. & Breton, J. (1988) *Proc. Natl. Acad. Sci. USA* **85,** 8468–8472.
32. Vos, M. H., Lambry, J. C., Robles, S. J., Youvan, D. C., Breton, J. & Martin, J. L. (1991) *Proc. Natl. Acad. Sci. USA* **88,** 8885–8889.
33. Vos, M. H., Rappaport, F., Lambry, J. C. & Martin, J. L. (1993) *Nature (London)* **363,** 320–325.
34. Mäntele, W., Wollenweber, A., Rashwan, F., Heinze, J., Nabedryk, E., Berger, G. & Breton, J. (1988) *Photochem. Photobiol.* **47,** 451–455.
35. Breton, J. & Nabedryk, E. (1993) *Chem. Phys. Lett.* **213,** 571–575.
36. Mattioli, T. A., Williams, J. C., Allen, J. P. & Robert, B. (1994) *Biochemistry* **33,** 1636–1643.
37. Nabedyk, E. & Breton, J. (1994) *Biophys. J.* **66,** A272 (abstr.).
38. Walker, G. C., Maiti, S., Cowen, B. R., Moser, C. C., Dutton, P. L. & Hochstrasser, R. M. (1994) *J. Phys. Chem.* **98,** 5778–5783.